Carbohydrate Polymers 111 (2014) 908–917

Contents lists available at ScienceDirect

Carbohydrate Polymers

journal homepage: www.elsevier.com/locate/carbpol

pH-sensitive pullulan-based nanoparticle carrier for adriamycin to overcome drug-resistance of cancer cells

Hua Guo[a,1], Yuanyuan Liu[a,b,1], Yan Wang[b], Jing Wu[a,c], Xiaoying Yang[b], Rongshan Li[b], Yinsong Wang[b,*], Ning Zhang[a,b,**]

[a] Laboratory of Cancer Cell Biology, Tianjin Medical University Cancer Institute and Hospital, National Clinical Research Center for Cancer, Key Laboratory of Cancer Prevention and Therapy, Tianjin 300060, PR China
[b] School of Pharmacy, Tianjin Key Laboratory on Technologies Enabling Development of Clinical Therapeutics and Diagnostics (Theranostics) & Research Center of Basic Medical Science, Tianjin Medical University, No. 22 Qixiangtai Road, Heping District, Tianjin 300070, PR China
[c] Tianjin Third Central Hospital, No. 83 Jintang Road, Hedong District, Tianjin 300170, PR China

ARTICLE INFO

Article history:
Received 11 December 2013
Received in revised form 13 April 2014
Accepted 13 May 2014
Available online 29 May 2014

Keywords:
O-Urocanyl pullulan
pH-sensitive
Nanoparticle carrier
Drug resistance
Cancer

ABSTRACT

Urocanic acid was conjugated to pullulan to synthesize *O*-urocanyl pullulan (URPA) with degree of substitution (DS) of 8.2%. URPA nanoparticles prepared by dialysis method had spherical shapes and a mean diameter of 156.8 ± 16.8 nm. Adriamycin (ADR) was successfully loaded into URPA nanoparticles and exhibited pH-sensitive *in vitro* release property. MTT assay showed that ADR-loaded URPA (ADR/URPA) nanoparticles had a significant higher toxicity against drug resistant MCF-7/ADR cells than free ADR, and the reversal index reached up to 9.6. The results of flow cytometry and confocal microscopy showed that URPA nanoparticles efficiently enhanced accumulation and retention of ADR in MCF-7/ADR cells and successfully delivered ADR into cell nucleus. The reversal effect of ADR/URPA nanoparticles on the drug resistance of MCF-7/ADR cells was perhaps related with their cell entry and intracellular drug release mechanisms.

1. Introduction

Cancer is a deadly disease. Chemotherapy is always believed as one of the most effective cancer treatments in clinical. However, the survival rate of cancer patients has not improved significantly in the last three decades. Drug resistance is a main problem to influence the efficacy of chemotherapy during long-term treatment on cancers (Persidis, 1999; Yardley, 2013). In several molecular mechanisms of cancer drug resistance, overexpression of P-glycoprotein (P-gp) in cancer cells is one main reason to cause drug resistant. P-gp, encoded by a multidrug resistance gene (MDR1), is an efflux transporter that pumps drug out from cells into the apical solution (Kartner & Ling, 1983). Drug resistant cells also acquire enhanced detoxification activities which convert cancer drugs into non-toxic derivatives (Florea & Büsselberg, 2011; Gottesman, Fojo, & Bates, 2002; Stavrovskaya, 2000). Until now, many attempts to modulate MDR1 activity during chemotherapy have not obtained ideal results due to undesired toxicity and poor specificity (Choi, 2005; Fox & Bates, 2007; Li et al., 2012).

With the development of nanotechnology, more and more investigations have shown that nanoparticle carriers for chemotherapeutic drugs are likely to be effective approaches to overcome cancer drug resistance (Dong & Mumper, 2010; Gowda, Jones, Banerjee, & Robertson, 2013; Peer et al., 2007). Drug delivery nanosystems have many advantages for cancer treatments, including the increased drug stability *in vivo*, enhanced permeability and retention (EPR) effect, easy surface modification, multifunctional platform, environmental stimuli-responsive properties (Blanco, Kessinger, Sumer, & Gao, 2009; Kim, Lee, Oh, Gao, & Bae, 2008; Oh et al., 2009). Nanoparticles formed by supramolecular assembly of pH-sensitive functional groups such as imidazole group can produce structural changes and release cargoes in response to the extracellular or intracellualr tumor pH (pHe, pHi) (Na, Lee, & Bae, 2007; Lee, Gao, & Bae, 2008). Some pH-sensitive nanoparticles can realize the intracellular drug delivery by responding to the acidic endosome/lysosome environment. After cellular internalization *via* endocytosis, these nanoparticles can gradually swell or disassemble with protonation of imidazole

* Corresponding author. Tel.: +86 2283336631.
** Corresponding author at: Tianjin Medical University Cancer Institute and Hospital, Huanhuxi Road, Hexi District, Tianjin, 300060, PR China. Tel.: +86 222 351 9721; fax: +86 222 351 9721.
E-mail addresses: wangyinsong@tijmu.edu.cn (Y. Wang), zhangning@tijmu.edu.cn (N. Zhang).
[1] These authors contributed equally to this work.

http://dx.doi.org/10.1016/j.carbpol.2014.05.057
0144-8617/

groups at acidic pH, thus trigger the release of loaded drugs. At the same time, strongly cationic imidazole groups can interact with negatively-charged endosomal membranes, which induce influx of water and ions, and eventually bring about the endosome destabilization and the drug release. This intracellular drug delivery is very favorable for the reversal of cancer drug resistant by avoiding the export effect of P-gp (Bae, Fukushima, Harada, & Kataoka, 2003; Kim, Lee, Oh, Gao, & Bae, 2008).

In our previous reports, we have synthesized a novel pH-sensitive pullulan derivative (*O*-urocanyl pullulan, URPA) by conjugation of urocanic acid to pullulan. URPA exhibits amphiphilic property in the neutral and weak alkaline media, thus can form self-assembled nanoparticles at concentration larger than its critical aggregation concentration (CAC) through the hydrophobic interactions among urocanyl groups. In addition, urocanyl group has pH-induced hydrophilic-hydrophobic transition capability at the pH around its pKa (~6.5) (Wang et al., 2013) due to the presence of imidazole cycle. Thus, URPA nanoparticles also exhibit pH-sensitive property and can disassemble in weak acidic medium (Scheme 1). In view of its pH-sensitive property, we hypothesize that URPA nanoparticle system can be used as an effective drug carrier to overcome cancer drug resistance. In this study, adriamycin (ADR) was chosen as a model anticancer drug to be physically loaded into URPA nanoparticles, and its *in vitro* releases were studied in aqueous media with different pH values. The reversal effects of ADR-loaded URPA (ADR/URPA) nanoparticles on drug resistant MCF-7/ADR cells were also investigated using MTT assay, flow cytometry and confocal microscopy technologies.

2. Experimental details

2.1. Materials

Pullulan (molecular mass of 200 kDa) was purchased from Hayashibara Biochemical Laboratory, Inc. (Okayama, Japan). ADR·HCl was purchased from Hisun Pharmaceutical Co. Ltd (Zhejiang, China). Trans-urocanic acid was purchased from Chemical Industry Co., Ltd. (Tokyo, Japan). Dicyclohexyl-carbodiimide (DCC), 4-(dimethylamino) pyridine (DMAP), fluorescein 5-isothiocyanate (FITC), 4,6′-diamidino-2-phenylindole (DAPI, D9564), 2,3-bis (2-methoxy-4-nitro-5-sulfophenyl)-2H-tetrazolium-5-carboxanilide inner salt (MTT), and dimethyl sulfoxide (DMSO) were purchased from Sigma–Aldrich Co. (St. Loius, Missouri, USA). Anti-P-gp and anti-β-actin antibodies were purchased from Santa Cruz Biotechnology Inc. (Santa Cruz, CA, USA). Goat anti-rabbit IgG-horseradish peroxidase (HRP) was purchased from CoWin Bioscience Inc. (Beijing, China). All other chemical reagents were analytical grade and obtained from commercial sources.

2.2. Synthesis and characterization of URPA

URPA was synthesized by the method we previously reported (Wang et al., 2013). Briefly, 0.3 g of trans-urocanic acid was activated with DDC and DMAP (1.2 M equivalent) in 10 mL dried DMSO under stirring at room temperature for 2 h. 1.0 g of pullulan was dissolved in 20 mL dried DMSO and then added into above solution. The mixture was stirred for 48 h and then filtered though membrane to remove dicyclohexylurea precipitate. The obtained filtrate was rapidly poured into 500 mL of ethanol to produce a white precipitate. This precipitate was then collected, respectively washed with ethanol, acetone and diethyl ether, and finally vacuum dried to obtain URPA powder. FITC-labeled URPA (FITC-URPA) was also synthesized according to the previous method (Kaneo, Tanaka, Nakano, & Yamaguchi, 2001).

URPA was chemically characterized by infrared (IR) spectroscopy, proton nuclear magnetic resonance (^{1}H NMR) spectroscopy and the elemental analysis. For IR spectra, pullulan and URPA were pressed with KBr as small discs and then performed on a FT-IR spectrometer (Nicolet NEXUS 470-ESP, USA). For ^{1}H NMR spectra, pullulan and URPA were dissolved in DMSO-d6 and then recorded on a 400 MHz NMR spectrometer (Varian Unity-plus 400, Bruker Co., Germany). Degree of substitution (DS) of urocanyl group, defined as the percentage of urocanyl groups grafted with glucose units of pullulan, was calculated according to the following formula, in which the nitrogen content (C_N %) was determined by the elemental analysis.

$$\mathrm{DS(mol\%)} = \frac{161C_N}{28 - 121C_N} \times 100\% \quad (1)$$

In addition, the amphiphilic property of URPA was evaluated by the fluorescence probe method using pyrene as a probe according to our previous report (Wang et al., 2013), and its critical aggregation concentration (CAC) in deionized water was also determined at the same time (supplementary materials).

2.3. Preparation and characterization of URPA nanoparticles

Dialysis method we previously reported (Wang et al., 2013) was used to prepare URPA nanoparticles in this study. Typically, URPA (100 mg) was dissolved in 10 mL of DMSO and stirred overnight. Then, URPA solution was transferred into dialysis bag (molecular weight cutoff 12–14 kDa) and dialyzed against deionized water. After dialysis for 6 h with 3 exchanges, the obtained colloid solution was sonicated at 20 W with a pulse function (pulse on 2.0 s, pulse off 2.0 s) for 2 min, and subsequently freeze-dried to obtain URPA nanoparticle powder.

The particle size and size distribution was determined using the dynamic laser light scattering method. Briefly, URPA nanoparticle sample was dispersed in deionized water at concentration of 0.5 mg/mL and then measured with a particles size analyzer (90 Plus, Malvern S Long Bed, England) at 25 °C. At same time, zeta potential measurements were performed using a zeta potential analyzer (Malvern S long bed, England). The morphology of URPA nanoparticles was observed using transmission electron microscope (TEM). URPA nanoparticle dispersion with concentration of 0.5 mg/mL was dropped onto the carbon-coated 400 mesh copper grid. After air-drying, the copper grid was imaged using TEM instrument (HT-7700, Hitachi, Japan).

2.4. Drug loading and in vitro release studies

ADR-loaded URPA (ADR/URPA) nanoparticles were prepared using the same method of preparation of plain URPA nanoparticles. Briefly, ADR·HCl was stirred with 3.0 equiv of triethylamine (TEA) in DMSO overnight at room temperature, and then mixed with URPA (100 mg) at weight ratios of 1/10, 2/10 and 3/10 in 10 mL of DMSO. Next, the mixture solutions were processed as above described to prepare ADR/URPA nanoparticles. The sizes and size distributions of ADR/URPA nanoparticles were determined by the dynamic laser scattering technique, and the morphologies were observed by TEM. Drug loading contents and encapsulation efficiencies were determined by the following method we previously reported (Wang, Liu, Jiang, & Zhang, 2007). ADR/URPA nanoparticle sample was absolutely dissolved in 2% acetic acid solution. Then, the fluorescence intensity of ADR was measured using RF-4500 fluorescence spectrophotometer (Shimadzu, Kyoto, Japan) at excitation and emission wavelength of 470 and 585 nm, respectively. ADR-loaded FITC-URPA (ADR/FITC-URPA) nanoparticles were also prepared by the above method with ADR/FITC-URPA feed weight ratio of 2/10.

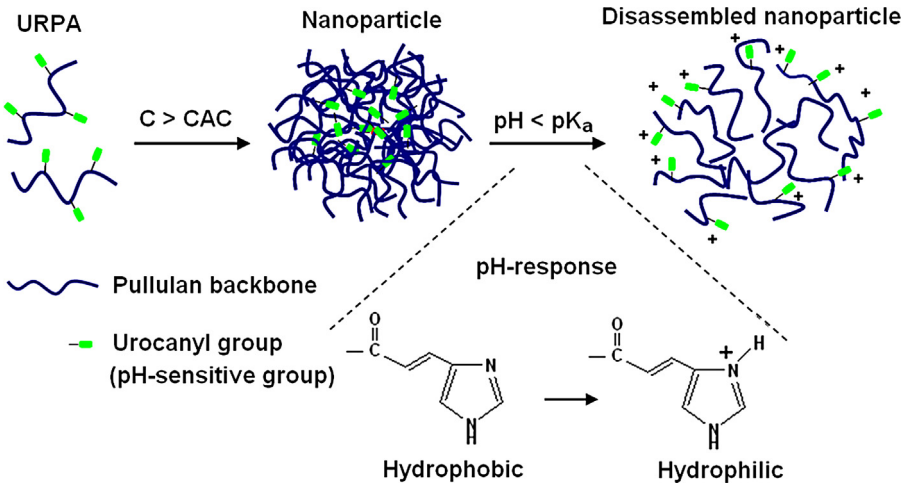

Scheme 1. The schematic representation of the formation and pH-response mechanisms of URPA nanoparticle.

Table 1
Characteristic parameters of ADR/URPA nanoparticles.

ADR/URPA[a] (w/w)	Size[b] (nm)	Polydispersity[b]	LC[c] (%)	EE[d] (%)	Zeta potential (mV)
1/10	198.7 ± 12.3	0.185 ± 0.016	8.59	90.5	−5.29 ± 0.63
2/10	236.3 ± 8.2	0.167 ± 0.012	13.8	79.6	−5.86 ± 0.38
3/10	320.8 ± 15.2	0.273 ± 0.028	19.2	70.1	−5.57 ± 0.35
4/10	439.8 ± 31.5	0.322 ± 0.015	19.8	49.5	−5.02 ± 0.43

[a] The feed weight ratio of ADR to URPA.
[b] The size and size distribution determined by the dynamic laser light scattering method.
[c] LC (drug loading content) = (weight of loaded ADR/weight of URPA nanoparticles) × 100%.
[d] EE (drug encapsulation efficiency) = (weight of loaded ADR/total weight of ADR) × 100%.

The dynamic dialysis method (Lee, Gao & Bae, 2008; Wang et al., 2013) was used to study the *in vitro* drug release property of ADR/URPA nanoparticles. Briefly, 50 mg of ADR/URPA nanoparticles were dispersed in 5 mL of deionized water and then transferred into dialysis bags (molecular weight cutoff 12–14 kDa, Millipore, Billerica, MA, USA). Next, nanoparticle dispersions were dialyzed against 100 mL of phosphate buffer solutions (PBS, 0.2 M solutions of Na_2HPO_4 and NaH_2PO_4, pH 7.4, 6.5 and 5.8) at 37 ± 0.2 °C in an air-bath shaker at 50 rpm. At predefined time intervals from 30 min to 36 h, 0.5 mL of release media were taken out and followed by adding 0.5 mL of the fresh release media. ADR concentrations of release media were measured by the fluorescence method as described above and ADR release rates were then calculated from ADR release amount to ADR total amount. In addition, the morphologies of ADR/URPA nanoparticles after drug release were observed by TEM.

2.5. Cell culture

Human breast cancer cell line MCF-7 and its ADR resistant cell line MCF-7/ADR were kindly gifted by Detroit Hospital (Detroit, Mich, USA). Cells were cultured at 37 °C under 5% CO_2 atmosphere in RPMI 1640 medium supplemented with 10% (v/v) fetal bovine serum (Hyclone, Logan, Utah, USA), 100 U/mL penicillin and 100 μg/mL streptomycin.

2.6. Cytotoxicity evaluation

To evaluate the reversal effect of ADR/URPA nanoparticles on cancer drug resistance, we preliminarily assessed their cytotoxicity against MCF-7 cells and drug resistant MCF-7/ADR cells by MTT assay, using free ADR as the control. Briefly, cells in their exponential growth phase were seeded onto 96-well culture plates at 5×10^3 cells/well and cultured for 24 h. The media were replaced with fresh culture media containing ADR/URPA nanoparticles or free ADR at different ADR concentrations. After 48 h of incubation, 20 μL of MTT reagent was added to each well and further incubated for 4 h. Next, the culture media were removed and 150 μL of DMSO were added to dissolve formazan crystals. The plates were then immediately read on a microplate reader (ELX800, Bio-tek EPOCH, Winooski, VT, USA) at 570 nm. Cell growth rates were expressed as a percentage of compared with the vehicle control. IC_{50}, ADR concentration required to inhibit cell growth by 50%, was determined from cell growth curve.

2.7. Cellular uptake and intracellular location of ADR/URPA nanoparticles

The uptakes of ADR/URPA nanoparticles in MCF-7 and MCF-7/ADR cells were measured by flow cytometry. Briefly, MCF-7 and MCF-7/ADR cells were placed in a 6-well culture plate and incubated to reach 80% confluence. Then, the culture media were replaced with fresh culture media containing free ADR or ADR/URPA nanoparticles at ADR concentration of 10 μg/mL. After incubation for a predefined time (10 min, 30 min, 1 h, 2 h, and 4 h), cells were washed with PBS, detached with 0.25% trypsin, and then centrifuged at 1000 rpm. After that, cells were suspended in PBS containing 0.1% bovine serum albumin (BSA) and then performed on a FACScalibur flow cytometer (Becton Dickinson, San Jose, CA, USA) for determination of ADR fluorescence intensities at 488 nm excitation and 575 nm emission.

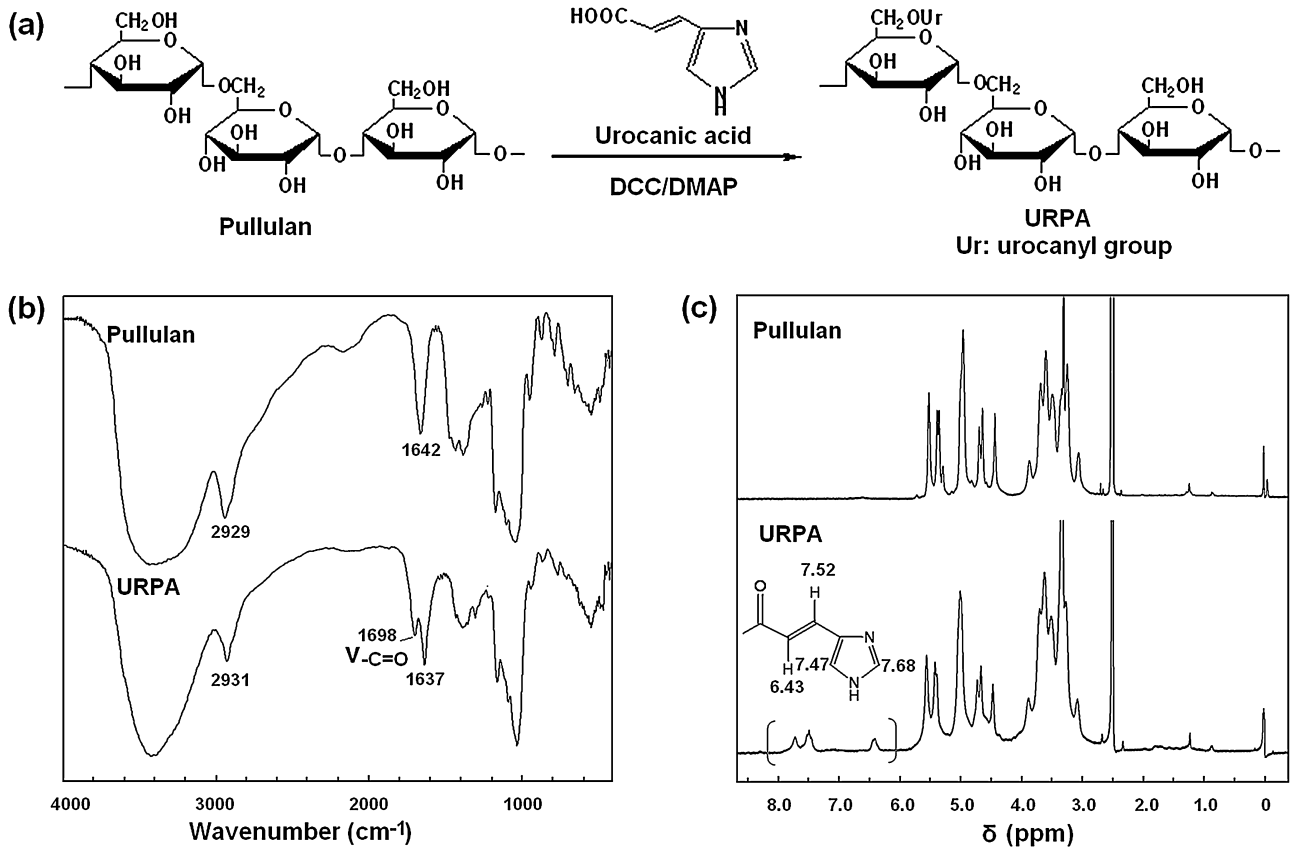

Fig. 1. Synthesis route of URPA (a), IR (b) and ^{1}H NMR spectra (c) of pullulan and URPA.

Intracellular distribution of ADR/FITC-URPA nanoparticles was evaluated by the confocal microscopy. Briefly, cells were seeded onto 12-well chambers with glass coverslip bottom at 1×10^5 cells/well and incubated overnight. Next, cells were cultured in serum-free media for 1 h and then further incubated in the culture media containing free ADR or ADR/FITC-URPA nanoparticles for a predefined time (10 min, 30 min, 1 h, 2 h, and 4 h). After that, cells were washed with PBS and fixed in 3.7% paraformaldehyde at 4 °C for 15 min. For location of nucleus, cells were stained with DAPI. Subsequently, cells were mounted in PBS containing 90% glycerol and imaged by a confocal microscope (FV1000, Olympus, Japan) in follow three fluorescence detection channels: red for ADR (excitation 488 nm, emission 575 nm), green for FITC (excitation 488 nm, emission 525 nm), and blue for DAPI (excitation 364 nm, emission 454 nm).

2.8. Western blot analysis

The expression levels of P-gp protein on the surfaces of MCF-7 and MCF-7/ADR cells were analyzed by western blotting. Briefly, total proteins were collected from MCF-7 or MCF-7/ADR cells and the protein concentrations were measured using BCA Protein Assay Kit. Total protein was denatured by boiling for 5 min. 50 μg of denatured proteins were resolved by SDS-polyacrylamide gel electrophoresis (SDS-PAGE) and then transferred onto PVDF membrane (Bio-Rad). Membranes were blocked with 5% dry skim milk (Bio-Rad) for 1 h at room temperature, and then probed with the primary antibodies against P-gp (1:2000) and β-actin (1:2000) overnight at 4 °C. After washing with TBST (Tween-20 1 mL, Tris-base 6.057 g, KCl 8.06 g, NaCl 6.057 g, deionized water 1 L, pH 8.0), the membranes were incubated with HRP-conjugated secondary antibody

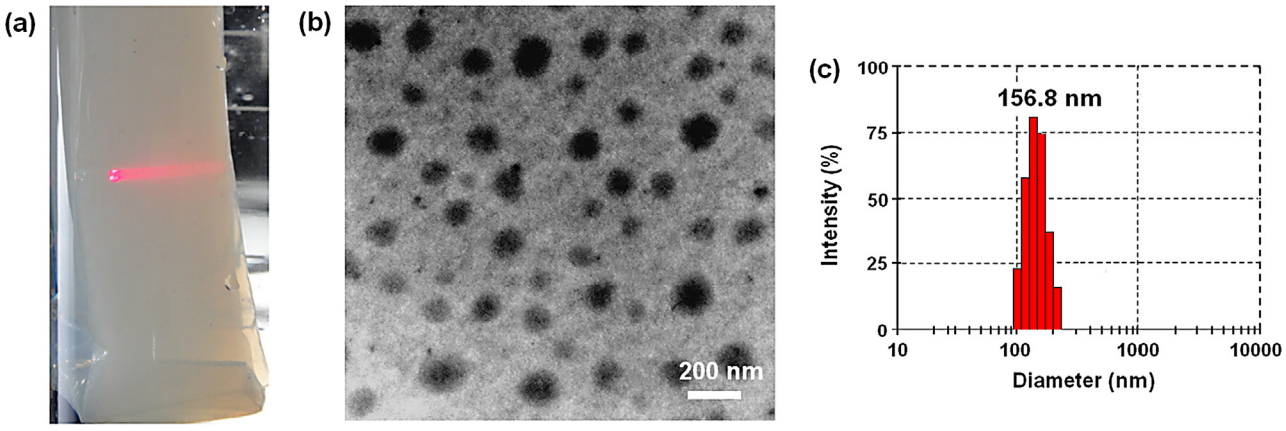

Fig. 2. Optical photograph (a), TEM image (b) and size distribution histogram (c) of URPA nanoparticles.

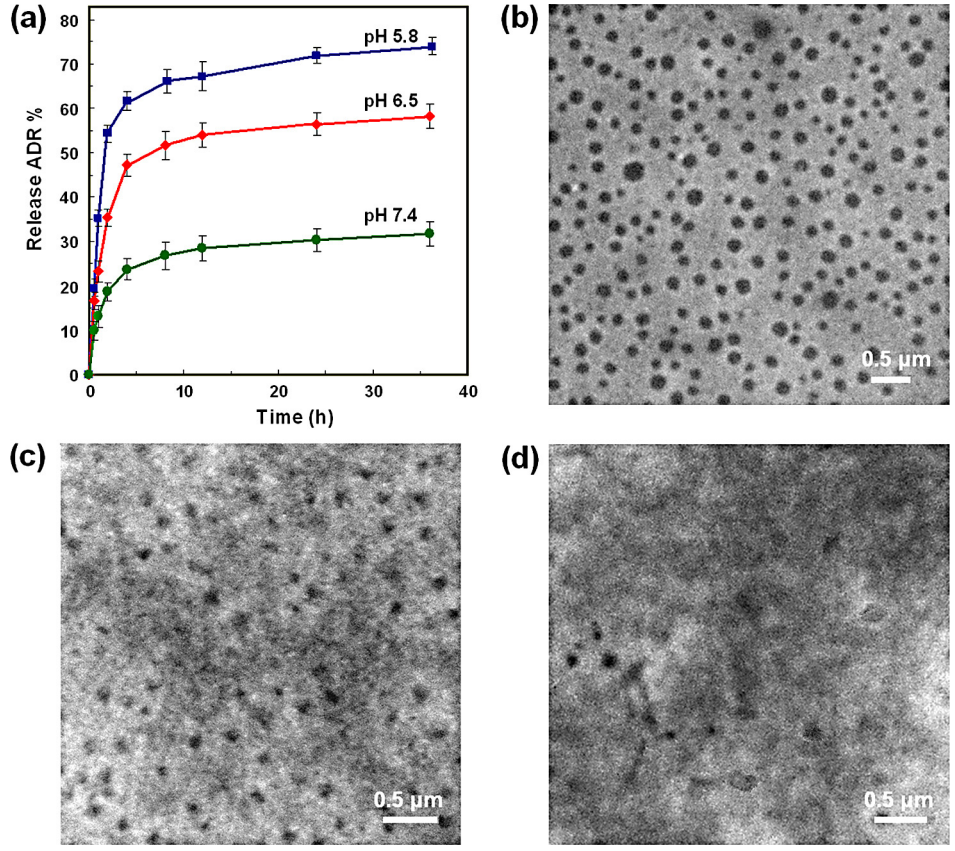

Fig. 3. *In vitro* drug release profiles at different pH values (a) and TEM images of ADR/URPA nanoparticles respectively at pH 7.4 (b), pH 6.5 (c) and pH 5.8 (d) after drug release.

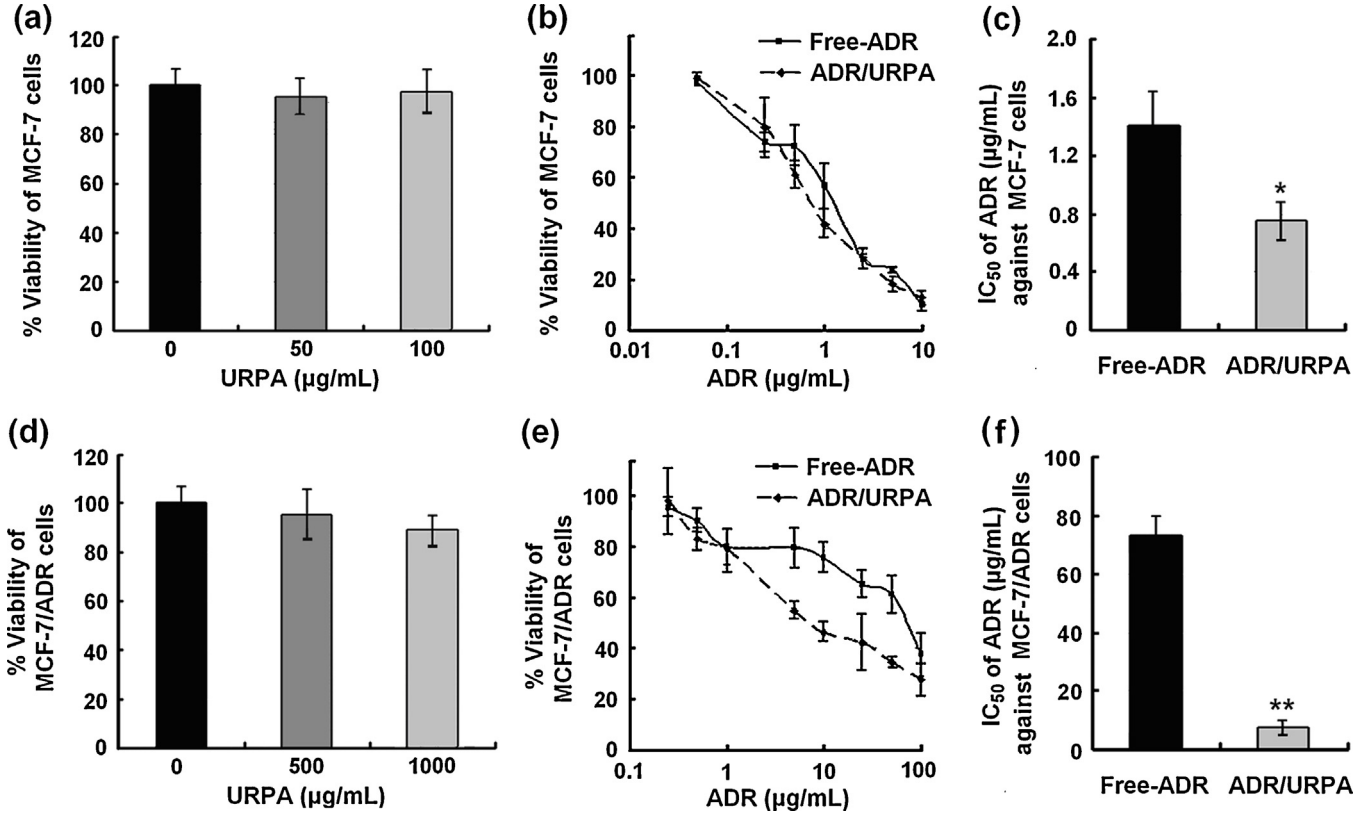

Fig. 4. Cytotoxicity assessments by MTT assay in MCF-7 and MCF-7/ADR cells. The inhibitory effects of plain URPA nanoparticles on the proliferations of MCF-7 (a) and MCF-7/ADR cells (d). Cytotoxicities of free ADR and ADR/URPA nanoparticles in MCF-7 (b) and MCF-7/ADR cells (e). The comparison of IC_{50} values of free ADR and ADR/URPA nanoparticles respectively for MCF-7 (c) and MCF-7/ADR cells (f). Data are mean ± standard deviation for 3 separate experiments. $^{*}P < 0.05$ and $^{**}P < 0.01$ in comparison to free ADR.

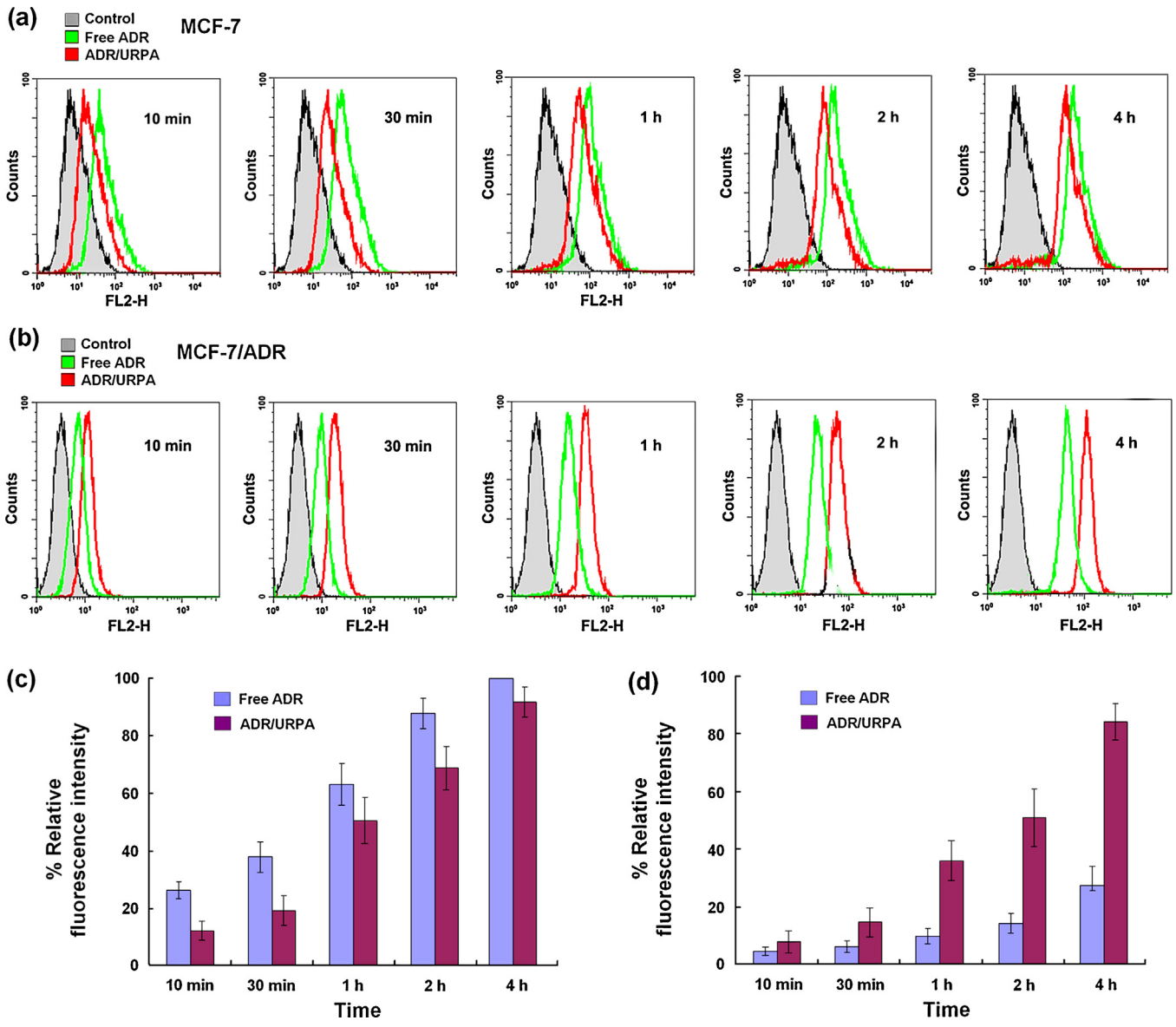

Fig. 5. The cellular uptake of free ADR and ADR/URPA nanoparticles. Fluorescence profiles measured by flow cytometry of MCF-7 (a) and MCF-7/ADR cells (b) treated with free ADR and ADR/URPA nanoparticles for 10 min to 4 h. The comparisons of the uptakes of free ADR and ADR/URPA nanoparticles in MCF-7 (c) and MCF-7/ADR cells (d), and the fluorescence intensity of free ADR in MFC-7 cells at 1 h was designated as 100%.

(1:5000) at 37 °C for 1 h, and then washed with TBST again. Western ECL Substrate (Bio-Rad) was used to visualize protein bands and the intensity of signals was analyzed using Image J densitometry software (National Institutes of Health, Bethesda, Maryland, USA).

2.9. Statistical analysis

All data are presented as mean ± standard deviation (SD) of at least three independent experiments. Statistical analysis was performed using one-way ANOVA and $P < 0.05$ was considered statistically significant.

3. Results and discussion

3.1. Synthesis and characterization of URPA

URPA was synthesized by conjugating trans-urocanic acid to pullulan backbone using DCC/DMAP mediated esterification method (Fig. 1a). Chemical structure of URPA was characterized by IR and ^{1}H NMR spectroscopy. In IR spectrum of URPA (Fig. 1b), the stretching vibrations of C=O and C=N in urocanyl group appeared respectively at 1698 and 1637 cm^{-1}. According to the previous report (Peng, Peng, Bian, Xu, & Sun, 2011), the peak at 1642 cm^{-1} in pullulan IR spectrum was attributed to the H–O–H bending of H_2O, which significantly reduced and overlapped with the C=N stretching peak at 1637 cm^{-1} in IR spectrum of URPA. In addition, the characteristic proton chemical shifts of vinyl and imidazole ring in urocanyl group were clearly observed at 6.0–8.0 ppm in ^{1}H NMR spectrum of URPA and the assignment of these chemical shifts are shown in Fig. 1c. The above results suggested that urocanic acid was successfully grafted onto pullulan backbone through ester bond. The nitrogen content determined by the elemental analysis was 1.33% (w/w), thus DS of urocanyl group calculated according to Formula 1 was 8.2%. URPA exhibited amphiphilic property and its CAC was 6.8×10^{-2} mg/mL, which was determined by the fluorescence probe method (supplementary materials).

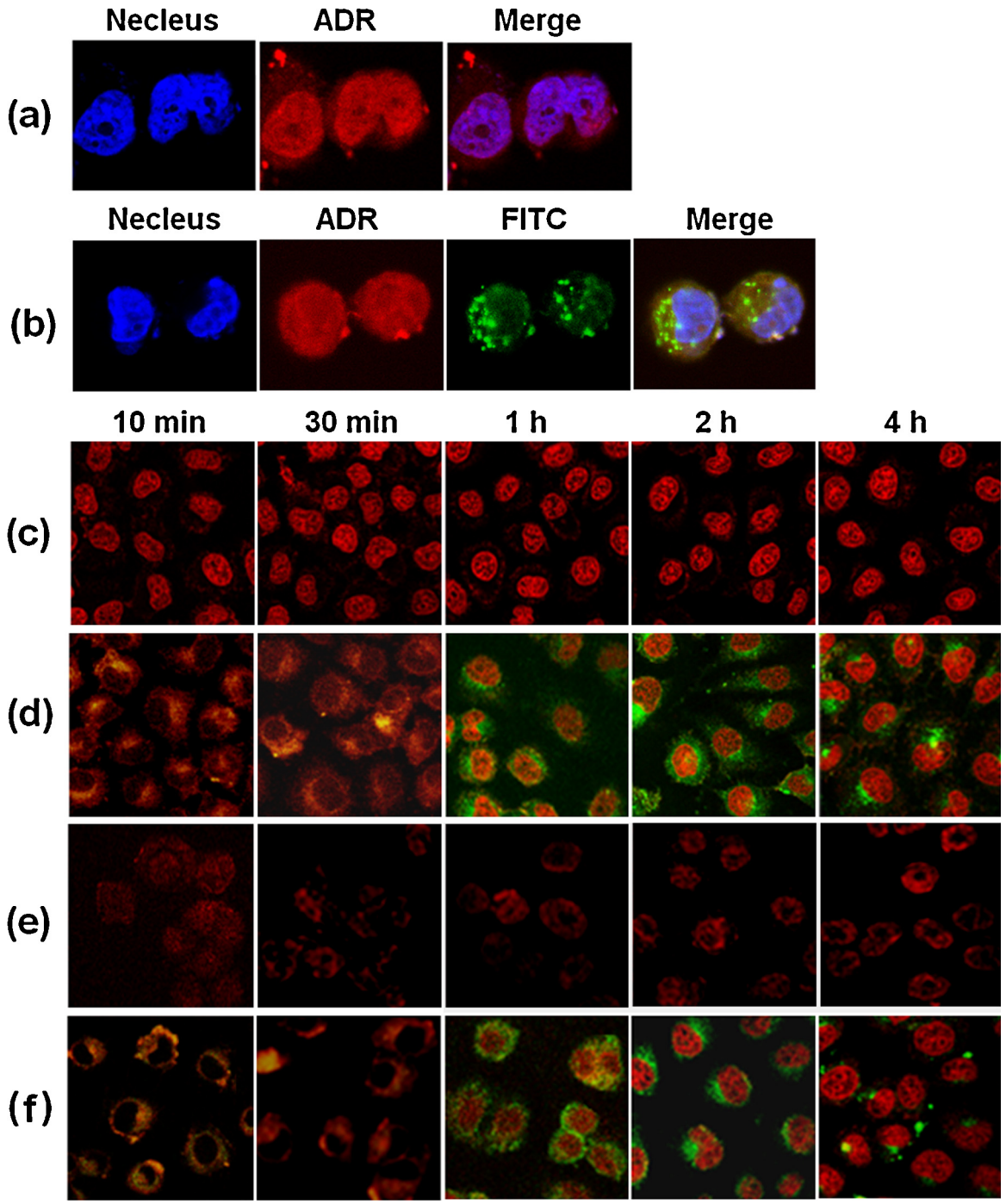

Fig. 6. Confocal microscopy images of MCF-7 and MCF-7/ADR cells with treatments of free ADR and ADR/FITC-URPA nanoparticles for 10 min to 4 h.
(a) The merge images taken from DAPI channel and ADR channel of MCF-7 cells with free ADR treatment for 2 h. (b) The merge images taken from DAPI channel, ADR channel and FITC channel of MCF-7/ADR cells with treatment of ADR/URPA nanoparticles for 2 h. (c) MCF-7 cells with free ADR treatment. (d) MCF-7 cells with treatment of ADR/URPA nanoparticles. (d) MCF-7/ADR cells with free ADR treatment. (e) MCF-7/ADR cells with treatment of ADR/URPA nanoparticles.

3.2. *Preparation and characterization of URPA nanoparticles*

In our previous report (Wang et al., 2013), the amphiphilic and pH-sensitive properties of URPA were evaluated by the fluorescence probe method. The results indicated that URPA exhibited amphiphilic property in neutral and weak alkaline media due to presence of both hydrophilic polysaccharide backbone and hydrophobic urocanyl groups. We thus deduced that URPA could form self-assembled nanoparticles through hydrophobic interactions among urocanyl groups in the aqueous media, like the other hydrophobically modified polysaccharides (Wang et al., 2008; Yinsong, Lingrong, Jian, & Zhang, 2007; Zhang, Wardwell, & Bader, 2013).

In this study, we prepared URPA nanoparticles using dialysis method. URPA was dissolved in DMSO and then dialyzed against water. The dialysis solution exhibited opalescence and Tyndall phenomenon was clearly observed (Fig. 2a), indicating that URPA formed nanoparticles in aqueous medium. After sonication, URPA nanoparticles exhibited regular spherical shape, monodispersity and relatively compact structure, shown in TEM image (Fig. 2b).

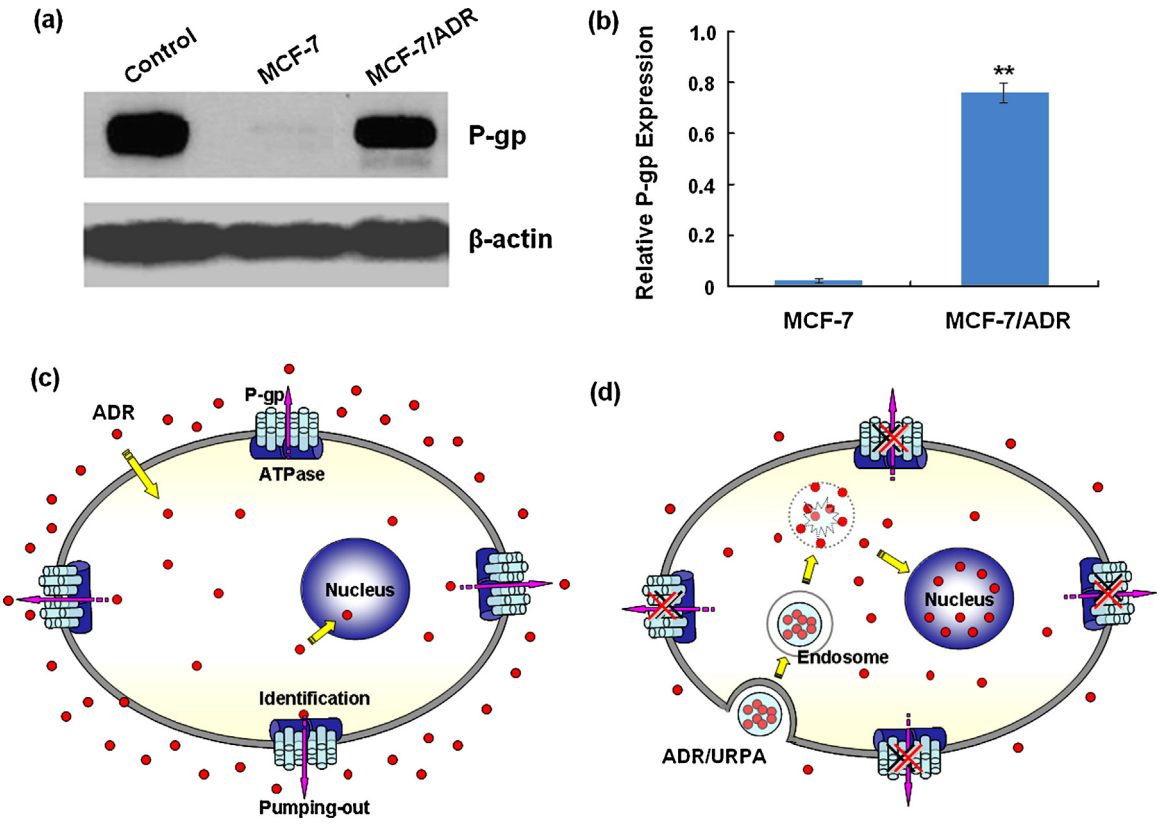

Fig. 7. Western blot analysis of P-gp expression in MCF-7/ADR cells and the illustration of reversal mechanism of ADR/URPA nanoparticles on drug resistance in MCF-7/ADR cells. (a) P-gp expressions in MCF-7 and MCF-7/ADR cells by western blot. (b) The densitometric analysis of P-gp. ** indicate $P < 0.01$. (c) The mechanism of drug resistance of MCF-7/ADR cells. (d) The reversal mechanism of ADR/URPA nanoparticles on drug resistance of MCF-7/ADR cells.

The size of URPA nanoparticles measured by the laser light scattering technique was 156.8 ± 16.8 nm and polydispersity index was 0.175 ± 0.019, indicating a uniform size distribution (Fig. 2c). Zeta potential of URPA nanoparticles was measured and its value was −4.78 ± 0.42 mV. According to the previous reports (Alexis, Pridgen, Molnar, & Farokhzad, 2008; Li & Huang, 2008; Tang et al., 2010; Wang et al., 2013), electrically neutral nanoparticles often exhibit the reduced uptake rate of macrophage phagocytosis system (MPS) and the prolonged circulation time, we thus deduced that URPA nanoparticles could be used as a sustained drug delivery carrier.

3.3. *Drug loading and in vitro release properties of URPA nanoparticles*

ADR was loaded into hydrophobic micro-domains of URPA nanoparticles through hydrophobic interactions. Table 1 shows the characterization of ADR/URPA nanoparticles. Obviously, ADR/URPA nanoparticles exhibited relatively high drug loading contents. With the feed weight ratio of ADR/URPA nanoparticles increasing from 1/10 to 4/10, drug loading content increased from 8.59% to 19.8%, but drug encapsulation efficiency decreased from 90.5% to 49.5%. At the same time, the size of ADR/URPA nanoparticles increased and the size distribution broadened, which suggested that the increase of drug loading content was likely to influence the stability of ADR/URPA nanoparticles. However, zeta potentials of ADR/URPA nanoparticles kept almost unchanged and exhibited the low absolute values. In view of the clinical application, such as small size, narrow size distribution, high drug loading content, and high drug encapsulation efficiency, 2/10 was believed the optimal feed ratio to prepared ADR/URPA nanoparticles.

URPA exhibited pH-sensitive behavior due to the presence of imidazole ring in the chemical structure of urocanyl group. Our previous report has confirmed its pH-sensitive behavior and the responding pH value determined by the fluorescence probe method was in the range of 7.0–6.0 (Wang et al., 2013). We thus believed ADR/URPA nanoparticles could realize the controlled drug release by responding to the environmental pH. The drug *in vitro* release profiles at different pH values are shown in Fig. 3a. At pH 6.5 and 5.8, URPA nanoparticles exhibited significantly higher drug release rates than that at pH 7.4. ADR amount released from URPA nanoparticles was only 30.5% at pH 7.4 over a 24 h period, but reached up to 56.3% and 72.1% at pH 6.5 and pH 5.8, respectively. However, free ADR exhibited rapid release rates in PBS solutions with different pH values, although a slightly slower release was observed at pH 7.4 than that at pH 5.8 and pH 6.5 (supplementary materials). The above results indicated that URPA nanoparticles used as the carrier for the antitumor drugs could realize pH-responsive drug release, which was favorable for drug escape from the acidic endosome/lysosome compartment after cellular internalization *via* endocytosis.

Next, TEM technique was used to observe morphological changes of ADR/URPA nanoparticles after drug releases at different pH values. As shown in Fig. 3b, ADR/URPA nanoparticles retained spherical shapes, monodispersity and compact structure at pH 7.4. However, disassembly of ADR/URPA nanoparticles was gradually observed as the medium pH decreased. For examples, nanoparticles showed irregular shapes, incompact structures and observably decreased size at pH 6.5 (Fig. 3c). When the medium pH further decreased to 5.8, these nanoparticles nearly disappeared and only polymer gel was observed (Fig. 3d). The above results indirectly confirmed pH-response mechanism of URPA nanoparticles we put forward in Scheme 1.

3.4. ADR/URPA nanoparticles overcame drug resistance of MCF-7/ADR cells

Cytotoxicities of free ADR and ADR/URPA nanoparticles were assessed in human breast cancer MCF-7 cells and drug resistant MCF-7/ADR cells using MTT assay. We firstly evaluated the cytotoxicity of plain URPA nanoparticles. As shown in Fig. 4a and d, URPA had no detectable inhibitory effects on the proliferations of MCF-7 and MCF-7/ADR cells in the used concentration range, which was consistent with our previous report (Wang et al., 2013). Due to drug resistance of MCF-7/ADR cells, free ADR exhibited a decreased cytotoxicity in MCF-7/ADR cells compared to MCF-7 cells (Fig. 4b and e), and its IC_{50} value significantly increased at the same time (Fig. 4f). The resistance index, defined as the ratio between IC_{50} values of ADR for MCF-7/ADR cells (73.2 ± 6.3 μg/mL) and for MCF-7 cells (1.4 ± 0.24 μg/mL), was high to 52.3. In both MCF-7 and MCF-7/ADR cells, ADR/URPA nanoparticles showed relatively higher cytotoxicities than free ADR (Fig. 4b and e), and IC_{50} values were 0.75 ± 0.13 μg/mL (Fig. 4c) and 7.6 ± 2.63 μg/mL respectively for MCF-7 and MCF-7/ADR cells (Fig. 4f). The above results indicated that ADR/URPA nanoparticles efficiently overcame drug resistance of MCF-7/ADR cells. The reversal index, calculated as a ratio between IC_{50} values of free ADR and ADR/URPA nanoparticles, reached up to 9.6.

3.5. ADR/URPA nanoparticles enhanced drug uptake in MCF-7/ADR cells

Based on the intrinsic fluorescence of ADR, the uptakes of free ADR and ADR/URPA nanoparticles in MCF-7 and MCF-7/ADR cells were evaluated by the flow cytometry. The fluorescence profiles and kinetic analysis (relative fluorescence intensity versus time) are plotted in Fig. 5. Free ADR rapidly entered MCF-7 cells through the passive diffusion (Fig. 5a). If the fluorescence intensity of free ADR in MCF-7 cells at 4 h was designated as 100%, the cellular uptake of free ADR exceeded 60% at 1 h (Fig. 5c). ADR/URPA nanoparticles exhibited the evidently lower uptakes in MCF-7 cells compared to free ADR, especially during the first 1 h (Fig. 5a and c), implying that ADR could not be completely transported into MCF-7 cells by loading of URPA nanoparticles. On the contrary, ADR/URPA nanoparticles significantly enhanced the drug uptake in MCF-7/ADR cells compared to free ADR. For example, the uptake of free ADR in MCF-7/ADR cells was only 27.5% at 4 h, whereas the cellular uptake of ADR/URPA nanoparticles reached up to 86.2% at the same time (Fig. 5d), which indicated that ADR was efficiently retained in MCF-7/ADR cells by loading of URPA nanoparticles. We believed this is the main reason of ADR/URPA nanoparticles to overcome the drug resistance of MCF-7/ADR cells.

3.6. URPA nanoparticles effectively delivered ADR to enter the nucleus of MCF-7/ADR cells

Next, we used the confocal microscopy to characterize the intracellular locations of free ADR and ADR/FITC-URPA nanoparticles in MCF-7 and MCF-7/ADR cells. Free ADR entered MCF-7 and MCF-7/ADR cells through the passive diffusion and was mainly located in the cell nucleus (Fig. 6a, c and e), due to the high affinity of ADR molecule for DNA (Kiyomiya, Matsuo, & Kurebe, 2001). Red fluorescence of free ADR in MCF-7/ADR cells was evidently weaker than that in MCF-7 cells, indicating that free ADR could not efficiently enter MCF-7/ADR cells due to drug resistance (Fig. 6c and e).

According to the previous reports (Gupta & Gupta, 2004; Liu, Jiao, Wang, Zhou, & Zhang, 2008; Na, Seong Lee, & Bae, 2003), polysaccharide-based nanoparticles entered cancer cells by endocytosis and the loaded drug was subsequently released. We thus evaluated drug release of ADR/FITC-URPA nanoparticles in cancer cells by the intracellular locations of red fluorescence of ADR and green fluorescence of FITC-URPA. In both MCF-7 and MCF-7/ADR cells, red fluorescence almost fully overlapped with green fluorescence during the first 30 min (Fig. 6d and f), indicating that ADR/URPA nanoparticles entered cells by the endocytosis without drug release. After 1 h, red fluorescence was separated from green fluorescence and mainly located in the cell nucleus (Fig. 6b, e and f), which implied that the loaded ADR was successfully released in the cytoplasm and then transferred into the cell nucleus. Moreover, the fluorescence intensity of ADR/URPA nanoparticles (Fig. 6f) located in the cell nucleus was significantly higher than that of free ADR (Fig. 6e). We could deduce from the above results that URPA nanoparticles used as the carrier for antitumor drugs could realize the intracellular drug delivery to exert therapeutic effects.

3.7. The possible mechanism of ADR/URPA nanoparticles to overcome drug resistance of MCF-7/ADR cells

Drug resistance is an obstacle to greater success with chemotherapy treatment. Patients receiving chemotherapy can develop resistance to previously effective drugs to the point that the drugs are no longer effective. Thus, how to overcome drug resistance is always a major problem in cancer chemotherapy. Overexpression of P-glycoprotein (P-gp), a membrane ATP-binding cassette transporter, is believed as the main resistant mechanism of cancer cells (Deeley, Westlake, & Cole, 2006; Kartner & Ling, 1983). We used western blotting to assess P-gp expressions in MCF-7 and MCF-7/ADR cells. As shown in Fig. 7a and b, P-gp expression in MCF-7/ADR cells was significantly higher than that in MCF-7 cells, suggesting overexpression of P-gp was the main mechanism of drug resistance in MCF-7/ADR cells. P-gp can use the energy released from ATP hydrolysis to pump a variety of anticancer drugs such as ADR out of the cells, which is defined as “export effect” (Fig. 7c). Avoidance of export effect of P-gp is a major strategy to overcome drug resistance in breast cancer cells (Ozben, 2006; Thomas & Coley, 2003). Many investigations focused on the usage of P-gp selective antagonisms, such as verapamil, cyclosporine, erythromycin, ketoconazole and tamoxifen (Hariharan, Gunda, Mishra, Pal, & Mitra, 2009; Summers, Moore, & McAuley, 2004; Thomas & Coley, 2003). However, these attempts are currently not satisfactory due to the high intrinsic toxicity of these compounds.

Advances in nanotechnology provide new approaches to overcome cancer drug resistance (Dong & Mumper, 2010; Gowda, Jones, Banerjee, & Robertson, 2013; Peer et al., 2007). In this study, we prepared a novel pH sensitive nanoparticle carrier for hydrophobic antitumor drugs and evaluated its potential to overcome cancer drug resistance. The results showed that ADR loaded by URPA nanoparticles was efficiently accumulated and retained in drug resistant MCF-7/ADR cells, thus exhibited greatly enhanced cytotoxicity. We believed the reversal effect of ADR/URPA nanoparticles on the drug resistance of MCF-7/ADR cells was related with their cell entry and intracellular drug release mechanisms. As shown in Fig. 7d, ADR/URPA nanoparticles could enter MCF-7/ADR cells through endocytosis, thus effectively avoid the export effect of P-gp expressed on the surface of MCF-7/ADR cells. In fact, many investigations have applied this strategy to successfully overcome cancer drug resistance (Milane, Ganesh, Shah, Duan, & Amiji, 2011; Wang et al., 2012; Yan et al., 2010). Furthermore, ADR/URPA nanoparticles could escape from the endosome/lysosome compartment and then release ADR into the cytoplasm by responding to the acidic endosomal/lysosomal environment. During this intracellular drug delivery process, ADR/URPA nanoparticles exhibited obvious synergistic effects in both MCF-7 and MCF-7/ADR cells compared to free ADR (Fig. 4c and f). Currently, we cannot elucidate the

mechanism of this synergistic effect, but it is evidently favor to overcome cancer drug resistance.

4. Conclusion

In this study, we prepared a pH-sensitive pullulan-based nanoparticle carrier for ADR and investigated its reversal effect against drug-resistance of MCF-7/ADR cells. The results showed that URPA nanoparticles possessed high ADR loading capability and exhibited pH-sensitive *in vitro* ADR release. In addition, URPA nanoparticles significantly enhanced the cellular uptake of ADR in MCF-7/ADR cells and delivered ADR to the cell nucleus by avoiding the export effect of P-gp, thus could effectively overcome the drug resistance of MCF-7/ADR cells. In conclusion, URPA nanoparticles used as the carrier of chemotherapeutic drugs will favor the reversal of cancer drug resistance.

Acknowledgements

This project was supported by grant from the 973 Program (2011CB933100), National Natural Science Foundation of China (no. 81371671 and 81201646), and the special program of China Postdoctoral Science Foundation (201104308).

Appendix A. Supplementary data

Supplementary data associated with this article can be found, in the online version, at http://dx.doi.org/10.1016/j.carbpol.2014.05.057.

References

Alexis, F., Pridgen, E., Molnar, L. K., & Farokhzad, O. C. (2008). Factors affecting the clearance and biodistribution of polymeric nanoparticles. *Molecular Pharmaceutics*, *5*(4), 505–515.

Bae, Y., Fukushima, S., Harada, A., & Kataoka, K. (2003). Design of environment-sensitive supramolecular assemblies for intracellular drug delivery: Polymeric micelles that are responsive to intracellular pH change. *Angewandte Chemie International Edition*, *42*(38), 4640–4643.

Blanco, E., Kessinger, C. W., Sumer, B. D., & Gao, J. (2009). Multifunctional micellar nanomedicine for cancer therapy. *Experimental Biology and Medicine (Maywood, N.J.)*, *234*(2), 123–131.

Choi, C.-H. (2005). ABC transporters as multidrug resistance mechanisms and the development of chemosensitizers for their reversal. *Cancer Cell International*, *5*(1), 30.

Deeley, R. G., Westlake, C., & Cole, S. P. (2006). Transmembrane transport of endo-and xenobiotics by mammalian ATP-binding cassette multidrug resistance proteins. *Physiological Reviews*, *86*(3), 849–899.

Dong, X., & Mumper, R. J. (2010). Nanomedicinal strategies to treat multidrug-resistant tumors: Current progress. *Nanomedicine*, *5*(4), 597–615.

Florea, A.-M., & Büsselberg, D. (2011). Cisplatin as an anti-tumor drug: Cellular mechanisms of activity, drug resistance and induced side effects. *Cancers*, *3*, 1351–1371.

Fox, E., & Bates, S. E. (2007). Tariquidar (XR9576): A P-glycoprotein drug efflux pump inhibitor. *Expert Review of Anticancer Therapy*, *7*(4), 447–459.

Gowda, R., Jones, N. R., Banerjee, S., & Robertson, G. P. (2013). Use of nanotechnology to develop multi-drug inhibitors for cancer therapy. *Journal of Nanomedicine & Nanotechnology*, *4*(6), 1000184.

Gottesman, M. M., Fojo, T., & Bates, S. E. (2002). Multidrug resistance in cancer: Role of ATP-dependent transporters. *Nature Reviews Cancer*, *2*(1), 48–58.

Gupta, M., & Gupta, A. K. (2004). Hydrogel pullulan nanoparticles encapsulating pBUDLacZ plasmid as an efficient gene delivery carrier. *Journal of Controlled Release*, *99*(1), 157–166.

Hariharan, S., Gunda, S., Mishra, G. P., Pal, D., & Mitra, A. K. (2009). Enhanced corneal absorption of erythromycin by modulating P-glycoprotein and MRP mediated efflux with corticosteroids. *Pharmaceutical Research*, *26*(5), 1270–1282.

Kaneo, Y., Tanaka, T., Nakano, T., & Yamaguchi, Y. (2001). Evidence for receptor-mediated hepatic uptake of pullulan in rats. *Journal of Controlled Release*, *70*(3), 365–373.

Kartner, N., & Ling, V. (1983). Cell surface P-glycoprotein associated with multidrug resistance in mammalian cell lines. *Science*, *221*(4617), 1285–1288.

Kim, D., Lee, E. S., Oh, K. T., Gao, Z. G., & Bae, Y. H. (2008). Doxorubicin-loaded polymeric micelle overcomes multidrug resistance of cancer by double-targeting folate receptor and early endosomal pH. *Small*, *4*(11), 2043–2050.

Kiyomiya, K.-I., Matsuo, S., & Kurebe, M. (2001). Mechanism of specific nuclear transport of adriamycin the mode of nuclear translocation of adriamycin-proteasome complex. *Cancer Research*, *61*(6), 2467–2471.

Lee, E. S., Gao, Z., & Bae, Y. H. (2008). Recent progress in tumor pH targeting nanotechnology. *Journal of Controlled Release*, *132*(3), 164–170.

Li, S. D., & Huang, L. (2008). Pharmacokinetics and biodistribution of nanoparticles. *Molecular Pharmaceutics*, *5*(4), 496–504.

Li, H., Hui, L., Xu, W., Shen, H., Chen, Q., Long, L., et al. (2012). Modulation of P-glycoprotein expression by triptolide in adriamycin-resistant K562/A02 cells. *Oncology Letters*, *3*(2), 485–489.

Liu, Z., Jiao, Y., Wang, Y., Zhou, C., & Zhang, Z. (2008). Polysaccharides-based nanoparticles as drug delivery systems. *Advanced Drug Delivery Reviews*, *60*(15), 1650–1662.

Milane, L., Ganesh, S., Shah, S., Duan, Z. F., & Amiji, M. (2011). Multi-modal strategies for overcoming tumor drug resistance: Hypoxia, the Warburg effect, stem cells, and multifunctional nanotechnology. *Journal of Controlled Release*, *155*(2), 237–247.

Na, K., Lee, E. S., & Bae, Y. H. (2003). Adriamycin loaded pullulan acetate/sulfonamide conjugate nanoparticles responding to tumor pH: pH-dependent cell interaction, internalization and cytotoxicity in vitro. *Journal of Controlled Release*, *87*(1), 3–13.

Na, K., Lee, E. S., & Bae, Y. H. (2007). Self-organized nanogels responding to tumor extracellular pH: pH-dependent drug release and in vitro cytotoxicity against MCF-7 cells. *Bioconjugate Chemistry*, *18*, 1568–1574.

Oh, K. T., Baik, H. J., Lee, A. H., Oh, Y. T., Youn, Y. S., & Lee, E. S. (2009). The reversal of drug-resistance in tumors using a drug-carrying nanoparticular system. *International Journal of Molecular Sciences*, *10*(9), 3776–3792.

Ozben, T. (2006). Mechanisms and strategies to overcome multiple drug resistance in cancer. *FEBS Letters*, *580*(12), 2903–2909.

Peer, D., Karp, J. M., Hong, S., Farokhzad, O. C., Margalit, R., & Langer, R. (2007). Nanocarriers as an emerging platform for cancer therapy. *Nature Nanotechnology*, *2*(12), 751–760.

Peng, P., Peng, F., Bian, J., Xu, F., & Sun, R. (2011). Studies on the starch and hemicelluloses fractionated by graded ethanol precipitation from bamboo phyllostachys bambusoides f. shouzhu Yi. *Journal of Agricultural and Food Chemistry*, *59*(6), 2680–2688.

Persidis, A. (1999). Cancer multidrug resistance. *Nature Biotechnology*, *17*(1), 94–95.

Stavrovskaya, A. (2000). Cellular mechanisms of multidrug resistance of tumor cells. *Biochemistry (Moscow)*, *65*(1), 95–106.

Summers, M. A., Moore, J. L., & McAuley, J. W. (2004). Use of verapamil as a potential P-glycoprotein inhibitor in a patient with refractory epilepsy. *The Annals of Pharmacotherapy*, *38*(10), 1631–1634.

Tang, H. B., Li, L., Chen, H., Zhou, Z. M., Chen, H. L., Li, X.-M., et al. (2010). Stability and in vivo evaluation of pullulan acetate as a drug nanocarrier. *Drug Delivery*, *17*(7), 552–558.

Thomas, H., & Coley, H. M. (2003). Overcoming multidrug resistance in cancer: An update on the clinical strategy of inhibiting p-glycoprotein. *Cancer Control: Journal of the Moffitt Cancer Center*, *10*(2), 159.

Wang, Y., Chen, H., Liu, Y., Wu, J., Zhou, P., Wang, Y., et al. (2013). pH-sensitive pullulan-based nanoparticle carrier of methotrexate and combretastatin A4 for the combination therapy against hepatocellular carcinoma. *Biomaterials*, *34*, 7181–7190.

Wang, Y., Guo, M., Lu, Y., Ding, L. Y., Ron, W. T., Liu, et al. (2012). Alpha-tocopheryl polyethylene glycol succinate-emulsified poly(lactic-co-glycolic acid) nanoparticles for reversal of multidrug resistance in vitro. *Nanotechnology*, *23*, 495103.

Wang, Y. S., Jiang, Q., Li, R. S., Liu, L. L., Zhang, Q. Q., Wang, Y. M., et al. (2008). Self-assembled nanoparticles of cholesterol-modified O-carboxymethyl chitosan as a novel carrier for paclitaxel. *Nanotechnology*, *19*(14), 145101.

Wang, Y. S., Liu, L. R., Jiang, Q., & Zhang, Q. Q. (2007). Self-aggregated nanoparticles of cholesterol-modified chitosan conjugate as a novel carrier of epirubicin. *European Polymer Journal*, *43*(1), 43–51.

Yan, Y., Ochs, C. J., Such, G. K., Heath, J. K., Nice, E. C., & Caruso, F. (2010). Bypassing multidrug resistance in cancer cells with biodegradable polymer capsules. *Advanced Materials*, *22*(47), 5324–5403.

Yardley, D. A. (2013). Drug Resistance and the role of combination chemotherapy in improving patient outcomes. *International Journal of Breast Cancer*, *2013*, 137414.

Yinsong, W., Lingrong, L., Jian, W., & Zhang, Q. (2007). Preparation and characterization of self-aggregated nanoparticles of cholesterol-modified O-carboxymethyl chitosan conjugates. *Carbohydrate Polymers*, *69*(3), 597–606.

Zhang, N., Wardwell, P. R., & Bader, R. A. (2013). Polysaccharide-based micelles for drug delivery. *Pharmaceutics*, *5*(2), 329–352.